Research Article | Vol. 28, No. 22 / 26 October 2020 / Optics Express 33619
Optics EXPRESS

Topological converter for high-efficiency coupling between Si wire waveguide and topological waveguide

HIBIKI KAGAMI,[1,4] TOMOHIRO AMEMIYA,[1,2,5] SHOU OKADA,[1] NOBUHIKO NISHIYAMA,[1,2] AND XIAO HU[3]

[1]*Department of Electrical and Electronic Engineering, Tokyo Institute of Technology, Tokyo 152-8552, Japan*
[2]*Institute of Innovative Research (IIR), Tokyo Institute of Technology, Tokyo 152-8552, Japan*
[3]*WPI-MANA, National Institute for Materials Science, Ibaraki 305-0044, Japan*
[4]*kagami.h.aa@m.titech.ac.jp*
[5]*amemiya.t.ab@m.titech.ac.jp*

Abstract: Replacing part of a conventional optical circuit with a topological photonic system allows for various controls of optical vortices in the optical circuit. As an underlying technology for this, in this study, we have realized a topological converter that provides high coupling efficiency between a normal silicon wire waveguide and a topological edge waveguide. After expanding the waveguide width while maintaining single-mode transmission from the Si wire waveguide, the waveguides are gradually narrowed from both sides by using a structure in which nanoholes with C_6 symmetry are arranged in a honeycomb lattice. On the basis of the analysis using the three-dimensional finite-difference time-domain method, we actually fabricated a device in which a Si wire waveguide and a topological edge waveguide were connected via the proposed topological converter and evaluated its transmission characteristics. The resulting coupling efficiency between the Si wire waveguide and the topological edge waveguide through the converter was –4.49 dB/taper, and the coupling efficiency was improved by 5.12 dB/taper compared to the case where the Si wire waveguide and the topological edge waveguide were connected directly.

1. Introduction

Tracing the topology of electronic systems in topological insulators and Weyl semimetals into photon systems is called '*topological photonics* [1]' and has rapidly progressed in recent years. The methods for expressing a topological phase in the field of photonics can be largely classified into three categories, namely an approach that makes use of time-reversal symmetry-breaking induced by a magneto-optical effect [2–5], a Floquet-like approach with periodic modulation in both space and time domains [6–9], and a time-reversal invariance approach using the spatial symmetry of an internal structure [10,11]. In particular, for a typical photonic structure of the third approach in which multiple dielectrics having C_6 symmetry are arranged in a honeycomb lattice, unprecedented optical phenomena can be realized because the unit cell has a higher degree of freedom in that configuration than that of a conventional photonic crystal whose unit cell comprises one dielectric.

The most well-known phenomenon is the topological edge state created by the aforementioned photonic structure, which enables the propagation of optical vortices in optical circuits [12–16]. The optical vortex carries the orbital angular momentum (OAM) of light and can be used to multiplex signals by assigning each signal to a light wave of different momentum. Even though the optical vortex is expected to be a large-capacity transmission technology in the future [17–22], conventional waveguide devices used in optical communication basically operate in TE/TM

#398421 https://doi.org/10.1364/OE.398421
Journal © 2020 Received 26 May 2020; revised 28 Aug 2020; accepted 31 Aug 2020; published 23 Oct 2020

Optics EXPRESS

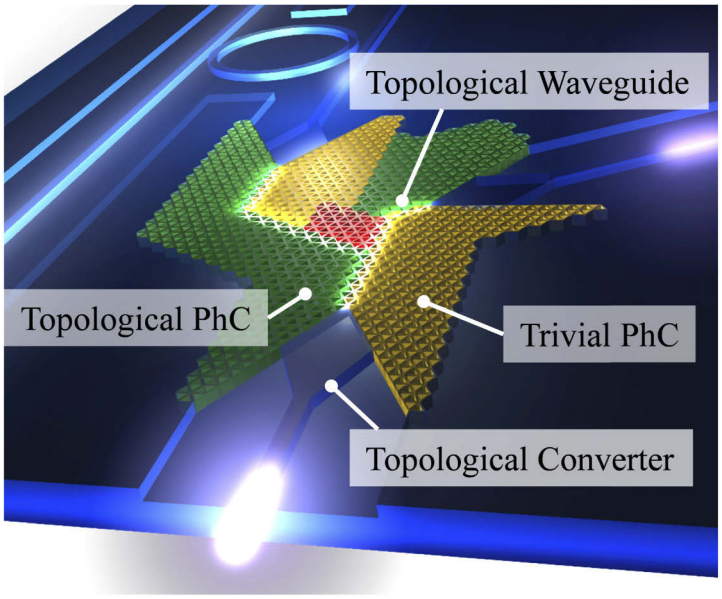

Fig. 1. TPICs: Topological photonic integrated circuits. By replacing part of the conventional optical circuit with a topological photonic system, various controls including optical vortex propagation can be performed in the optical circuit.

mode light and are not suitable for optical vortex transmission [23–26]. For this reason, as shown in Fig. 1, we are aiming to perform various optical vortex controls in optical circuits by replacing parts of conventional optical circuits with topological photonic systems (TPICs: topological photonic integrated circuits) [27]. In TPICs, possible applications include lasers that excite specific optical vortex modes and optical vortex multiplexer/demultiplexer that can operate without any power consumption. The former one can be realized by using a III-V semiconductor air bridge topological structure [28], and the latter one can be realized by using a designed topological edge waveguide that allows a specific optical vortex mode [29].

One of the indispensable elements of TPICs mentioned above is the highly efficient coupling from a normal waveguide to a topological edge waveguide (efficient conversion from TE/TM mode to optical vortex mode). However, it is difficult to realize appropriate coupling because the shape of the normal waveguide is significantly different from that of the topological edge waveguide [30–32] formed at the interface between a trivial photonic structure and a topological photonic structure.

In this study, we have proposed a topological converter to realize high-efficiency coupling between a silicon wire waveguide and a topological edge waveguide. After outlining the proposed device including operation principles, we analyzed the propagation characteristics using the finite-difference time-domain (FDTD) method (Section 2). On the basis of the theoretical analysis, we then fabricated the actual device and investigated its coupling characteristics (Section 3). The details are described in the following sections.

2. Overview and theoretical analysis of the topological converter

2.1. Outline of the proposed topological converter including operation principles

Figure 2(a) shows a schematic of the topological converter. In this study, we consider creating the TPICs on a silicon-on-insulator (SOI) wafer that is normally used in optical circuits. First, the waveguide width is gradually increased while maintaining single-mode transmission from

Optics EXPRESS

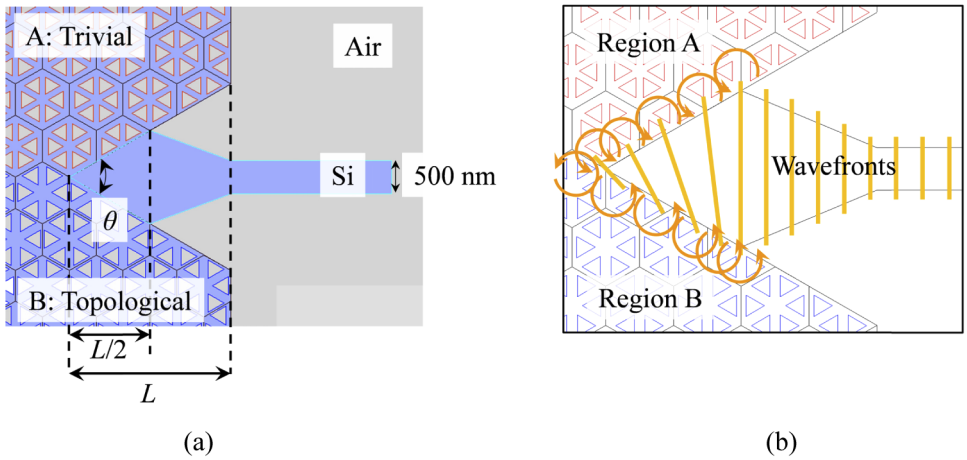

Fig. 2. (a) Overview of the proposed topological converter. (b) Operating principles of the proposed topological converter: The two sides of the waveguide (Regions A and B) are a trivial photonic structure and a topological photonic structure, respectively. There is a slight misalignment in the dielectric placement, which causes the equiphase plane of the TE/TM mode to incline with propagation.

the Si wire waveguide. After that, by using a structure in which nanoholes with C_6 symmetry are arranged in a honeycomb lattice [33–35], the waveguide is gradually narrowed from both sides to achieve high-efficiency coupling to the topological edge waveguide. Here, each side of the waveguide (region A and B in Fig. 2(a)) has a trivial photonic structure or a topological photonic structure, and the dielectrics on both sides are displaced by half a lattice with each other. This causes a wavefront tilt of the TE/TM mode depending on the propagation distance (Fig. 2(b)). Finally, when the wavefront tilt matches the optical vortex mode, the device achieves high-efficiency coupling to the zigzag topological edge waveguide.

2.2. *Design of the photonic structure used in the topological converter*

We first designed the photonic structure to place in each domain. In this study, for a photonic structure having a $\mathbb{Z}2$ topological phase, we adopted a structure where triangular nanoholes with C_6 symmetry are arranged in a honeycomb lattice on a SOI wafer (see Fig. 3(a)). In this structure, we assumed that a Si core layer with a film thickness of 220 nm, which is normally used in silicon photonics circuits, was sandwiched between a 1.5-μm-thick SiO_2 cladding and an air cladding. In a simulation, the period of the honeycomb lattice a_0 was fixed to 800 nm, and the distance r from the center of the honeycomb lattice to the center of the nanohole, and the length l of one side of the nanohole, were used as parameters for analysis.

Figure 3(b) shows the TE-mode band diagrams for each structure calculated by using the 3-dimensional plane wave expansion (PWE) method. By gradually changing the parameters from $r = 243$ nm, $l = 245$ nm to $r = 291$ nm, $l = 250$ nm, the electromagnetic mode of the p-wave and d-wave was inverted near the center of the Brillouin zone, causing the transition from a trivial photonic band to a topological photonic band (see [31] for more information about p-wave and d-wave). As two photonic structures used in the topological converter must be a typical trivial photonic structure and a topological photonic structure, respectively, the parameters in regions A and B shown in Fig. 2(a) were set to $r = 243$ nm, $l = 245$ nm and $r = 291$ nm, $l = 250$ nm, respectively. Here, the center of the bandgap of each photonic structure corresponds to the wavelength of the input light (= 1550 nm).

Optics EXPRESS

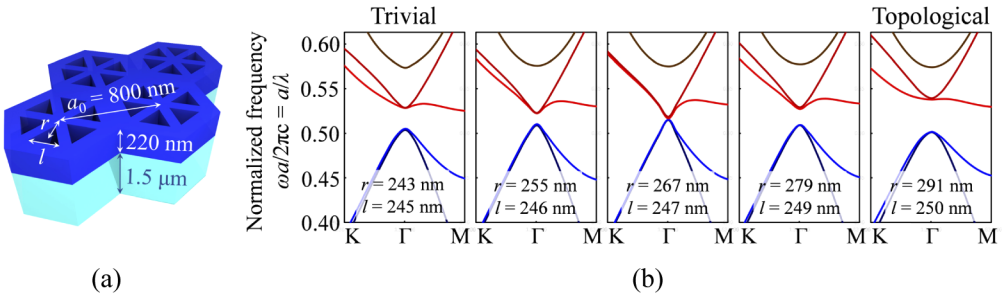

Fig. 3. (a) Photonic structure used in the topological converter. (b) TE-mode Band diagrams for each structure calculated using the plane wave expansion (PWE) method: By gradually increasing r and l, the electromagnetic mode of the p-wave and d-wave underwent band inversion near the Γ point of the band diagram, causing the transition from a structure with a trivial photonic band to a structure with a topological photonic band.

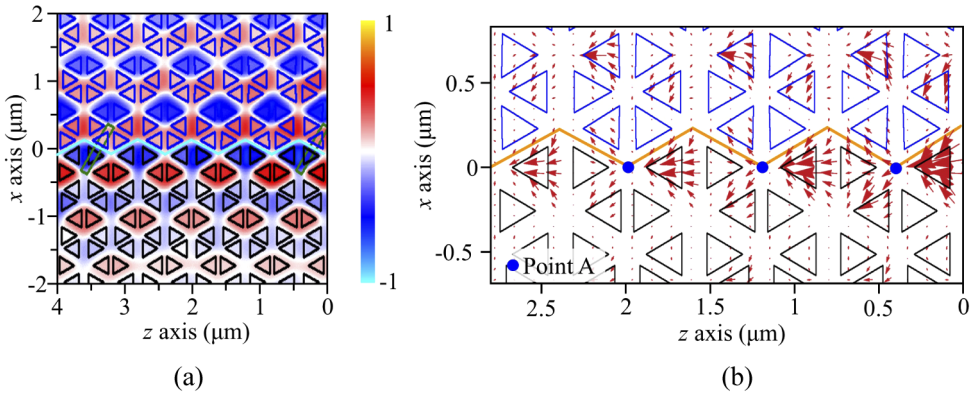

Fig. 4. Propagation characteristics of the topological transmission line analyzed by the FDTD method. (a) Electromagnetic field mode distribution (H_y) of the optical vortex mode excited by the topological transmission line at a certain point (b) Energy flow ($\vec{E} \times \vec{H}$) of the optical vortex mode excited by the topological transmission line at a certain point.

2.3. *Positioning of input and output ends of the topological edge waveguide in the topological converter*

In this section, we determine the position of the input and output ends of the topological edge waveguide used in the topological converter. Unlike the TE/TM mode in the Si wire waveguides, the direction of the energy vector is non-uniform for the optical vortex mode in the topological edge waveguide. For this reason, the input and output ends of the topological edge waveguide need to be placed in an appropriate position to achieve high-efficiency coupling.

Using the photonic structure designed in the previous section, we analyzed the propagation characteristics of the topological edge waveguide formed at the interface between the trivial photonic structure and the topological photonic structure. Figure 4 shows the results calculated by the three-dimensional FDTD method. Figures 4(a) and 4(b) show the electromagnetic field distribution (H_y) and energy flow ($\vec{E} \times \vec{H}$) of the optical vortex mode excited in the topological edge waveguide at a certain time. In Fig. 4(a), we can see that the p-wave and d-wave are equally mixed in the propagating optical vortex mode, which means the optical vortex modes of $l = 1$ and $l = 2$ are mixed at a ratio of 1:1. This is because the bandgap center wavelength of all photonic structures that form this device is the same as that of the input light, and the transition ratio of

Optics EXPRESS

the electromagnetic mode ($p\pm$, $d\pm$) is the same. As the energy flow at this time is concentrated in the z direction at the position A, as shown in Fig. 4(b), the input and output ends of the topological edge waveguide were placed in these positions. This enables the high-efficiency coupling between the Si wire waveguide and the zigzag topological edge waveguide.

2.4. Propagation characteristics and coupling efficiency of the topological converter

Next, using the structure established in Sections 2.2 and 2.3, we designed the whole structure of the topological converter shown in Fig. 2(a) and investigated its propagation characteristics. In the simulation, we changed the distance L between the Si wire waveguide and input end of the topological edge waveguide, and the narrowing angle θ formed by two photonic structures. With respect to the distance L, the Si wire waveguide was gradually widened with a length of $L/2$, and then narrowed with a length of $L/2$ by two photonic structures arranged on both sides of the waveguide. In addition, the angle θ was set to 30° or 60° in consideration of the fact that the photonic structure has nanoholes having C_6 symmetry arranged in a honeycomb lattice.

Figure 5 shows a typical propagation mode field near the topological converter, calculated by the three-dimensional FDTD method (assuming $L = 4.0$ μm and $\theta = 45°$ as parameters). Figure 5(a) shows the magnetic field distribution (H_y) viewed from directly above the device, and Figs. 5(b) and 5(c) show cross-sectional views of the magnetic field distribution (H_y) along a–a' and b–b' in Fig. 5(a), respectively. For comparison, propagation analysis was also performed for a device in which a Si waveguide was directly connected to a topological edge waveguide without using the topological converter (see Figs. 5(d)–5(f)). From Figs. 5(a)–5(c), TE-mode light propagating in the Si wire waveguide was efficiently coupled to the optical vortex mode of the topological edge waveguide while suppressing reflection and scattering through the topological converter. On the other hand, as evident from Figs. 5(d)–5(f), in the case without the topological converter, significant reflection and scattering occurred at the interface due to the large mode mismatch between the Si wire waveguide and topological edge waveguide.

In order to calculate the coupling efficiency of the topological converter, we analyzed its propagation characteristics using the model shown in Fig. 6(a). The analysis model consists of [Si wire waveguide – topological converter – topological edge waveguide – topological converter – Si wire waveguide], and the transmission intensity was calculated by changing the length of the topological edge waveguide (i.e. number of cells of the honeycomb lattice). In the simulation, input and output ports were placed in the Si wire waveguides. Figure 6(b) shows the coupling efficiency of the topological converter analyzed by changing the parameters L and θ. Figure 6(c) also shows the coupling efficiency of the topological converter as a function of θ, where L is fixed at 4.0 μm, which corresponds to the white dashed line in Fig. 6(b). These results indicated that there is a significant improvement in coupling efficiency when the topological converter is introduced to the device, compared to when the Si wire waveguide and the topological edge waveguide were connected directly. Furthermore, the parameter L had a greater effect on the coupling efficiency than the parameter θ, and the device with $\theta = 45°$ showed an increase in coupling efficiency of 1.8 dB and 4.1 dB compared to the devices with $\theta = 30°$ and 60°, respectively. Finally, a maximum coupling efficiency of –0.4 dB/taper was obtained for the topological converter with parameters of $L = 4.0$ μm and $\theta = 45°$ (here, the propagation loss of the topological edge waveguide was 0.25 dB/cell).

Figure 6(d) shows the coupling efficiency as a function of wavelength, for the topological converter with parameters of $L = 4.0$ μm and $\theta = 45°$. When the structural parameters of the topological converter were optimized for appropriate mode matching between the Si wire waveguide and the topological edge waveguide, the wavelength dependence was almost constant from 1540 nm to 1560 nm. This means the wavelength dispersion of the device is extremely small in this wavelength range.

Optics EXPRESS

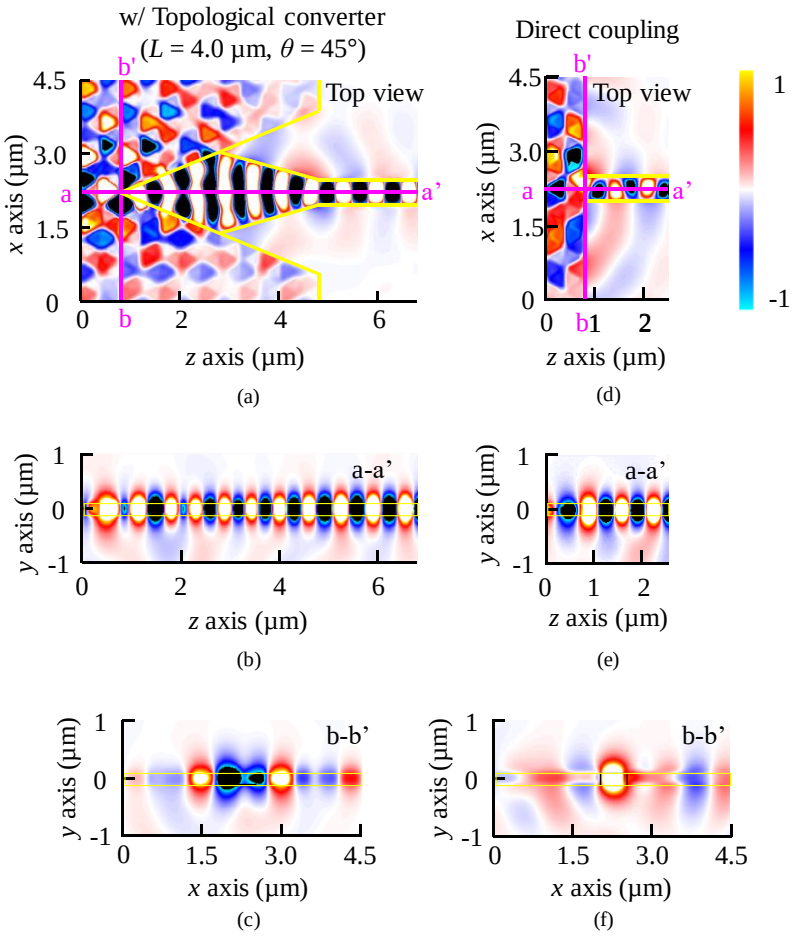

Fig. 5. Typical propagation mode near the topological converter, calculated by the FDTD method (assuming parameters of $L = 4.0$ μm, $\theta = 45°$ for the topological converter): (a) Magnetic field mode distribution (H_y) from right above the device. (b)(c) Magnetic field mode distribution (H_y) of the a-a' and b-b' cross-sections. (d)-(f) Results of analyzing the device in which the Si wire waveguide is directly connected to the topological transmission line without a topological converter.

Optics EXPRESS

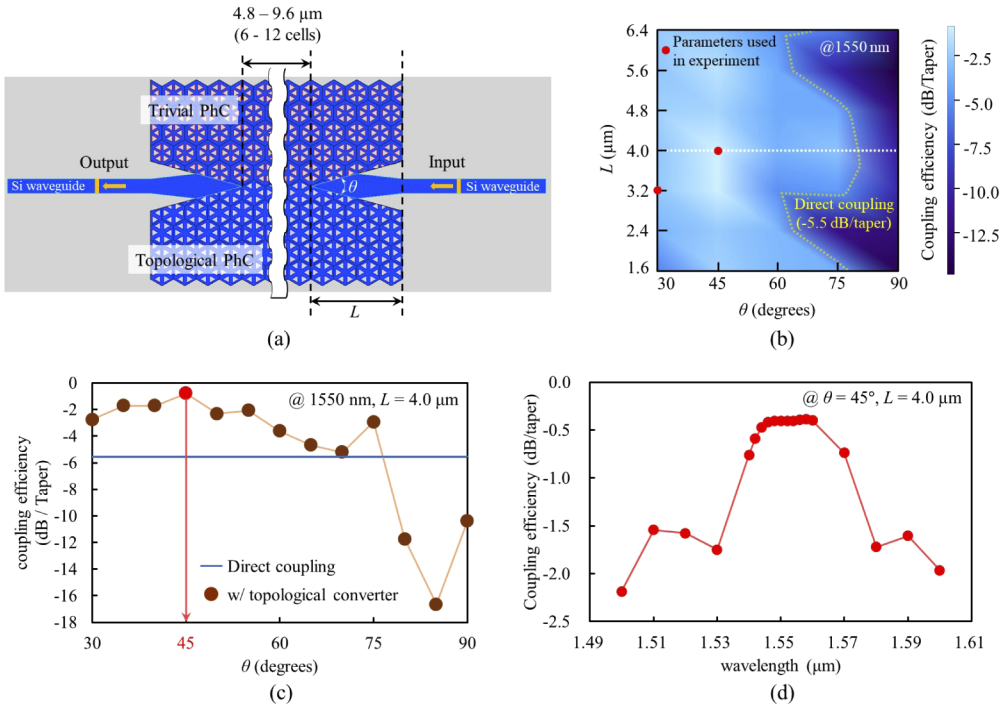

Fig. 6. (a) An analytical model to calculate the coupling efficiency of the topological converter (the input/output ports are placed on the flanking Si wire waveguides). (b) Coupling efficiency of the topological converter as a function of the parameters L and θ. (c) Coupling efficiency of the topological converter as a function of θ (L is fixed at 4.0 μm), which corresponds to the white dashed line in Fig. 6(b). (d) Wavelength dependence of coupling efficiency of the topological converter with parameters of $L = 4.0$ μm and $\theta = 45°$.

3. Fabrication and evaluation of the topological converter

Based on the design described in Section 2, we fabricated a device in which a Si wire waveguide was connected to a topological edge waveguide via a topological converter and measured characteristics of the device. First, ZEP520A (film thickness: 500 nm) was coated onto a SOI substrate (Si core thickness: 220 nm, SiO_2 clad thickness: 1.5 μm). After that, a device pattern was formed by electron-beam lithography and inductively coupled plasma reactive ion etching (ICP-RIE) with CF_4-SF_6 mixed gas (mixing ratio 8:1). We ensured that the parameters of the trivial photonic structure and the topological photonic structure would be $r = 243$ nm, $l = 245$ nm and $r = 291$ nm, $l = 250$ nm, respectively. In this study, two types of devices with parameters of $(L, \theta) = (3.2$ μm, 30°), (4.0 μm, 45°) were prepared. In addition, for comparison with the above device, we also prepared a reference device on the same substrate whereby the Si wire waveguide was connected directly to the topological edge waveguide, without a topological converter.

Figures 7(a) and 7(b) show scanning electron microscope (SEM) images of the fabricated device near the topological converter and the topological edge waveguide, respectively. Figures 7(a) and 7(b) indicated that each parameter of the device had a value close to the design dimensions mentioned in Section 2. Furthermore, Figs. 7(c) and (d) show SEM images along a–a' and b–b' in Fig. 7(a), respectively. In this study, the upper cladding layer was air for both the Si wire waveguide and the topological edge waveguide.

We measured the propagation characteristics of the device for 1550-nm-band incident light. Light from a tunable laser (17 dBm) was transferred into and out of the device using lensed-fiber

Optics EXPRESS

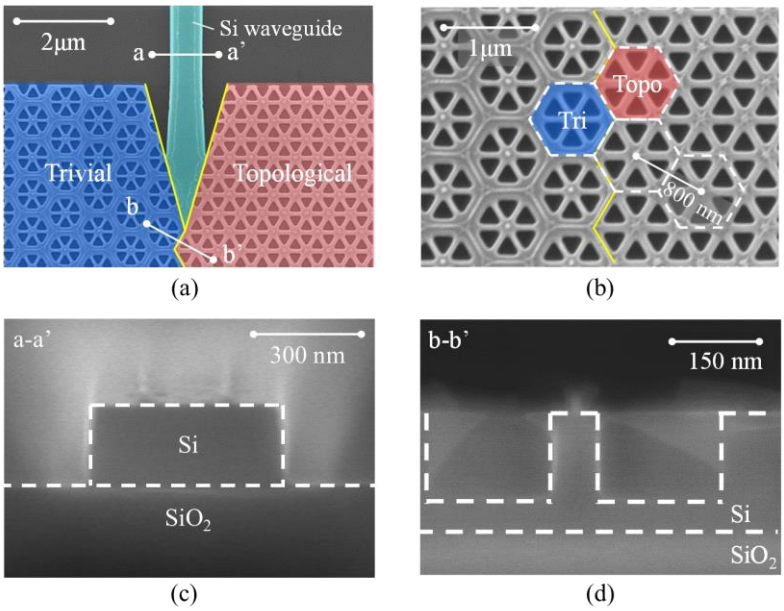

Fig. 7. (a)(b) Scanning electron micrographs (SEM) taken near the topological converter in the fabricated device. (c)(d) SEM of the a-a' and b-b' cross-sections.

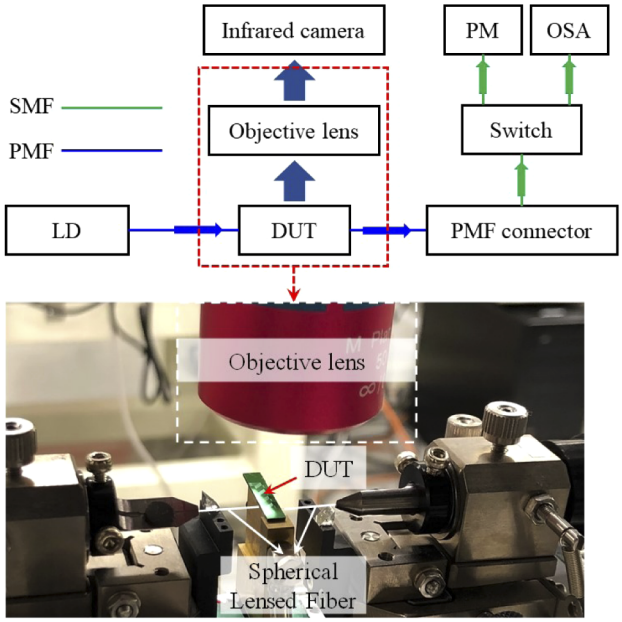

Fig. 8. Experimental system to calculate the coupling efficiency of the topological converter.

Optics EXPRESS

couplers (See Fig. 8). The intensity of output light from the device was measured using the optical spectrum analyzer and the power meter. At the same time, an Infrared camera (Hamamatsu Photonics: C14041-10U) was used to observe the upward-scattered light from the device.

Figures 9(a)–9(c) show Infrared camera images at various incident wavelengths, and Figs. 9(d)–(f) show band diagrams of assumed photonic structures. In the wavelength range of 1520–1560 nm, as incident light from the Si wire waveguide was transmitted to the trivial and topological photonic structures, light energy was estimated to be above the bandgap of each photonic structure (Figs. 9(a) and 9(d)). As the wavelength of the incident light varied to the long-wavelength side, light leakage to each photonic structure was suppressed when reaching the vicinity of the bandgap edge (Figs. 9(b) and 9(e)). When the wavelength of the incident light ultimately reached

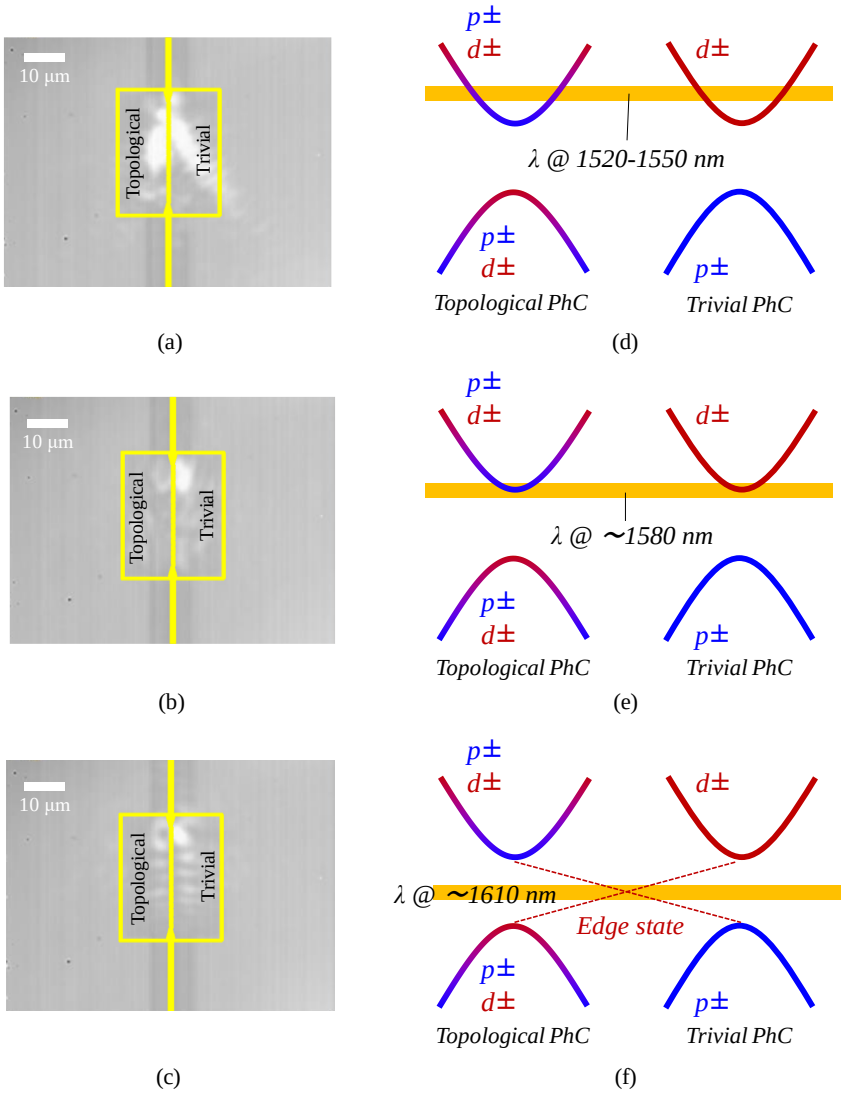

Fig. 9. Infrared camera images at each wavelength and the band diagrams of each photonic structure estimated from these results. (a)(d) Wavelength of incident light: 1520–1560 nm. (b)(e) Wavelength of incident light: 1580 nm. (c)(f) Wavelength of incident light: 1610 nm.

Optics EXPRESS

1610 nm, we were able to observe the propagation of light from the Si wire waveguide to the topological edge waveguide (Figs. 9(c) and 9(f)). In Fig. 9, the center wavelength of the bandgap deviates from the value set at first (= 1550 nm). This is because the nanoholes in each photonic structure were 190-nm-deep equilateral triangles with rounded corners, while in the theoretical analysis, they were assumed to be ideal equilateral triangles with a depth of 220 nm.

Figure 10 shows the propagation characteristics of the device at an incident light wavelength of 1610 nm. In this experiment, we prepared devices in which the length of the topological edge waveguide was changed from 8 μm (10 cells) to 28 μm (35 cells). From the intercept of the approximate line in Fig. 10, the coupling efficiency w/ the topological converter was estimated to be -5.88 dB/taper for the parameters of $(L, \theta) = (3.2\ \mu m, 30°)$ and -4.49 dB/taper for the parameters of $(L, \theta) = (4.0\ \mu m, 45°)$. On the other hand, the coupling efficiency w/o the topological converter was estimated to be -9.61 dB/taper. These results indicated that there is a significant improvement in coupling efficiency when the topological converter is introduced to the device. Although the coupling efficiency improved by the topological converter is presently smaller than that of the theoretical value, we believe that it would be possible to approach the theoretical value of –0.40 dB/taper through optimization of the fabrication process.

In addition, from the slope of the approximate line in Fig. 10, the propagation loss of the topological edge waveguide was -0.4 dB/cell in all cases. As mentioned in Section 1, it is ideal that most of the optical functions are performed in the conventional low-loss optical circuit and only the control related to the optical vortex is realized using the topological photonics system. Since the size of the topological photonic region seems to be about 10×10 um^2, the propagation loss of the topological edge waveguide is not a significant problem within such a scale.

Finally, we measured wavelength dependence of the topological converter with parameters of $L = 4.0\ \mu m$ and $\theta = 45°$. Figure 11 shows the result. The wavelength dependence was almost constant from 1590 nm to 1630 nm, which indicates that the wavelength dispersion of the device is extremely small in this wavelength range.

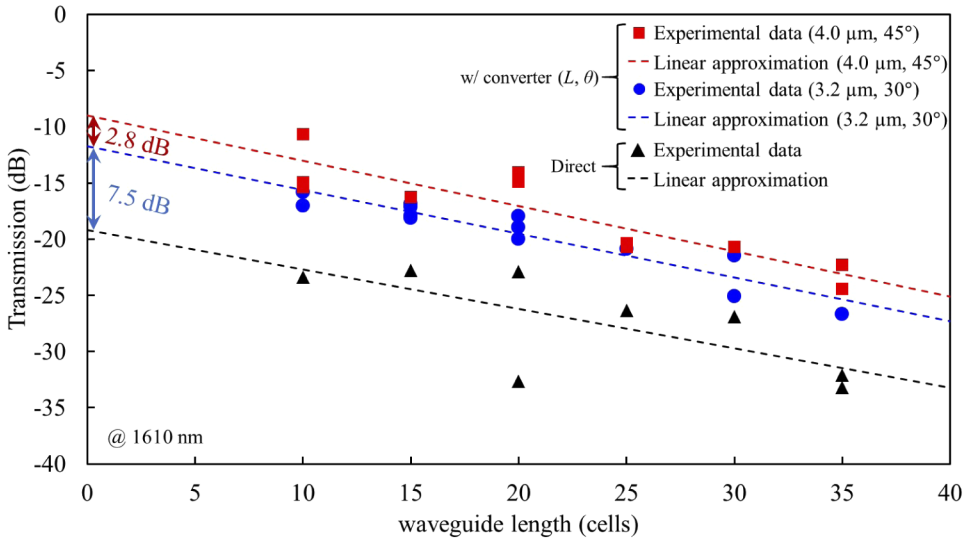

Fig. 10. Propagation characteristics of the device at incident light wavelength of 1610 nm: The coupling efficiency of the topological converter and the transmission loss of the topological transmission line itself were estimated by varying the length of the topological transmission line from 8 μm (10 cell) to 28 μm (35 cell), and comparing their transmission intensities.

Optics EXPRESS

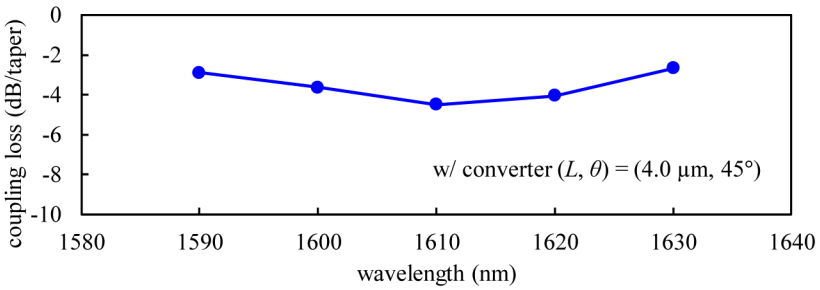

Fig. 11. Measured wavelength dependence of coupling efficiency of the topological converter with parameters of $L = 4.0$ μm and $\theta = 45°$.

4. Conclusion

Various optical vortex controls in optical circuits can be performed by replacing part of a conventional optical circuit with a topological photonic system. As an underlying technology for this, we have proposed a topological converter to realize high-efficiency coupling between a Si wire waveguide and a topological edge waveguide. In the topological converter, the waveguide width was first gradually increased while maintaining single-mode transmission from the Si wire waveguide. After that, by using a structure in which nanoholes with C_6 symmetry are arranged in a honeycomb lattice, the waveguide was gradually narrowed from both sides to achieve high-efficiency coupling to the topological edge waveguide.

As a result of analyzing the propagation characteristics of the device by the three-dimensional FDTD method, we found that introducing the topological converter led to significant improvements in coupling efficiency compared to when the Si wire waveguide was connected directly to the topological edge waveguide. Finally, we estimated that it would be possible to achieve a maximum coupling efficiency of –0.40 dB/taper with this device.

On the basis of simulation results, we actually fabricated a device on a SOI substrate, whereby the Si wire waveguide was connected to a topological edge waveguide via a topological converter. As a result, the coupling efficiency between the Si wire waveguide and the topological edge waveguide with and without the topological converter was –4.49 and –9.61 dB/taper, respectively (the coupling efficiency was improved by about 5.12 dB with the topological converter).

Funding

Ministry of Internal Affairs and Communications (182103111); Japan Society for the Promotion of Science (19H02193); Core Research for Evolutional Science and Technology (JPMJCR15N6, JPMJCR18T4).

Acknowledgments

We would like to thank Dr. S. Arai, Professor Emeritus of Tokyo Institute of Technology, for his advice and cooperation.

Disclosures

The authors declare no conflicts of interest.

References

1. T. Ozawa, H. M. Price, A. Amo, N. Goldman, M. Hafezi, L. Lu, M. C. Rechtsman, D. Schuster, J. Simon, O. Zilberberg, and I. Carusotto, "Topological Photonics," Rev. Mod. Phys. **91**(1), 015006 (2019).

Optics EXPRESS

2. Y. Poo, R. Wu, Z. Lin, Y. Yang, and C. T. Chan, "Experimental realization of self-guiding unidirectional electromagnetic edge states," Phys. Rev. Lett. **106**(9), 093903 (2011).
3. S. A. Skirlo, L. Lu, and M. Soljačić, "Multimode one-way waveguides of large Chern numbers," Phys. Rev. Lett. **113**(11), 113904 (2014).
4. S. A. Skirlo, L. Lu, Y. Igarashi, Q. Yan, J. D. Joannopoulos, and M. Soljačić, "Experimental observation of large Chern numbers in photonic crystals," Phys. Rev. Lett. **115**(25), 253901 (2015).
5. L. Lu, C. Fang, L. Fu, S. G. Johnson, J. D. Joannopoulos, and M. Soljačić, "Symmetry-protected topological photonic crystal in three dimensions," Nat. Phys. **12**(4), 337–340 (2016).
6. N. H. Linder, G. Refael, and V. Galitski, "Floquet topological insulator in semiconductor quantum wells," Nat. Phys. **7**(6), 490–495 (2011).
7. T. Kitagawa, E. Berg, M. Rudner, and E. Demler, "Topological characterization of periodically driven quantum systems," Phys. Rev. B **82**(23), 235114 (2010).
8. K. Fang, Z. Yu, and S. Fan, "Photonic Aharonov–Bohm effect based on dynamic modulation," Phys. Rev. Lett. **108**(15), 153901 (2012).
9. K. Fang, Z. Yu, and S. Fan, "Realizing effective magnetic field for photons by controlling the phase of dynamic modulation," Nat. Photonics **6**(11), 782–787 (2012).
10. R. O. Umucalılar and I. Carusotto, "Artificial gauge field for photons in coupled cavity arrays," Phys. Rev. A **84**(4), 043804 (2011).
11. M. Hafezi, E. A. Demler, M. D. Lukin, and J. M. Taylor, "Robust optical delay lines with topological protection," Nat. Phys. **7**(11), 907–912 (2011).
12. A. B. Khanikaev and G. Shvets, "Two-dimensional topological photonics," Nat. Photonics **11**(12), 763–773 (2017).
13. S. Barik, A. Karasahin, C. Flower, T. Cai, H. Miyake, W. DeGottardi, M. Hafezi, and E. Waks, "A topological quantum optics interface," Science **359**(6376), 666–668 (2018).
14. X.-T. He, E.-T. Liang, J.-J. Yuan, H.-Y. Qiu, X.-D. Chen, F.-L. Zhao, and J.-W. Dong, "A silicon-on-insulator slab for topological valley transport," Nat. Commun. **10**(1), 872 (2019).
15. N. Parappurath, F. Alpeggiani, L. Kuipers, and E. Verhagen, "Direct observation of topological edge states in silicon photonic crystals: Spin, dispersion, and chiral routing," Sci. Adv. **6**(10), eaaw4137 (2020).
16. P. D. Anderson and G. Subramania, "Unidirectional edge states in topological honeycomb-lattice membrane photonic crystals," Opt. Express **25**(19), 23293–23301 (2017).
17. T. Su, R. P. Scott, S. S. Djordjevic, N. K. Fontaine, D. J. Geisler, X. Cai, and S. J. B. Yoo, "Demonstration of free space coherent optical communication using integrated silicon photonic orbital angular momentum devices," Opt. Express **20**(9), 9396–9402 (2012).
18. N. Bozinovic, Y. Yue, Y. Ren, M. Tur, P. Kristensen, H. Huang, A. E. Willner, and S. Ramachandran, "Terabit-scale orbital angular momentum mode division multiplexing in fibers," Science **340**(6140), 1545–1548 (2013).
19. H. Huang, G. Xie, Y. Yan, N. Ahmed, Y. Ren, Y. Yue, D. Rogawski, M. J. Willner, B. I. Erkmen, K. M. Birnbaum, S. J. Dolinar, M. P. J. Lavery, M. J. Padgett, M. Tur, and A. E. Willner, "100 Tbit/s free-space data link enabled by three-dimensional multiplexing of orbital angular momentum, polarization, and wavelength," Opt. Lett. **39**(2), 197–200 (2014).
20. B. Guan, R. P. Scott, C. Qin, N. K. Fontaine, T. Su, C. Ferrari, M. Cappuzzo, F. Klemens, B. Keller, M. Earnshaw, and S. J. B. Yoo, "Free-space coherent optical communication with orbital angular momentum multiplexing/demultiplexing using a hybrid 3D photonic integrated circuit," Opt. Express **22**(1), 145–146 (2014).
21. Y. Wang, P. Zhao, X. Feng, Y. Xu, K. Cui, F. Liu, W. Zhang, and Y. Huang, "Integrated photonic emitter with a wide switching range of orbital angular momentum modes," Sci. Rep. **6**(1), 22512 (2016).
22. T. Amemiya, T. Yoshida, Y. Atsumi, N. Nishiyama, Y. Miyamoto, Y. Sakakibara, and S. Arai, "Orbital angular momentum MUX/DEMUX module using vertically curved Si waveguide," in *Optical Fiber Communication Conference (OFC) 2019*, OSA Technical Digest (Optical Society of America, 2019), paper M1C.7.
23. L. A. Coldren, S. C. Nicholes, L. Johansson, S. Ristic, R. S. Guzzon, E. J. Norberg, and U. Krishnamachari, "High performance InP-based photonic ICs—A tutorial," J. Lightwave Technol. **29**(4), 554–570 (2011).
24. R. Nagarajan, M. Kato, D. Lambert, P. Evans, S. Corzine, V. Lal, J. Rahn, A. Nilsson, M. Fisher, M. Kuntz, J. Pleumeekers, A. Dentai, H.-S. Tsai, D. Krause, H. Sun, K.-T. Wu, M. Ziari, T. Butrie, M. Reffle, M. Mitchell, F. Kish, and D. Welch, "Terabit/s class InP photonic integrated circuits," Semicond. Sci. Technol. **27**(9), 094003 (2012).
25. J. K. Doylend and A. P. Knights, "The evolution of silicon photonics as an enabling technology for optical interconnection," Laser Photonics Rev. **6**(4), 504–525 (2012).
26. P. P. Absil, P. Verheyen, P. De Heyn, M. Pantouvaki, G. Lepage, J. De Coster, and J. Van Campenhout, "Silicon photonics integrated circuits: a manufacturing platform for high density, low power optical I/O's," Opt. Express **23**(7), 9369–9378 (2015).
27. T. Amemiya, H. Kagami, K. Saito, N. Nishiyama, and S. Arai, "Topological Photonic Integrated Circuits for Controlling OAM light signal," Laser Photonics Rev. **13**(12), 1900087 (2019).
28. Z.-Q. Yang, Z.-K. Shao, H.-Z. Chen, X.-R. Mao, and R.-M. Ma, "Spin-Momentum-Locked Edge Mode for Topological Vortex Lasing," Phys. Rev. Lett. **125**(1), 013903 (2020).
29. T. Amemiya, K. Saito, H. Kagami, S. Okada, and X. Hu, "Topological photonic circuit," Patent application number 2019-151863.

Optics EXPRESS

30. Y. Yang, Y. Yamagami, X. Yu, P. Pitchappa, J. Webber, B. Zhang, M. Fujita, T. Nagatsuma, and R. Singh, "Terahertz topological photonics for on-chip communication," Nat. Photonics **14**(7), 446–451 (2020).
31. Y. Ota, F. Liu, R. Katsumi, K. Watanabe, K. Wakabayashi, Y. Arakawa, and S. Iwamoto, "Photonic crystal nanocavity based on a topological corner state," Optica **6**(6), 786–789 (2019).
32. H. Yoshimi, T. Yamaguchi, Y. Ota, Y. Arakawa, and S. Iwamoto, "Slow light waveguides in topological valley photonic crystals," Opt. Lett. **45**(9), 2648–2651 (2020).
33. L.-H. Wu and X. Hu, "Scheme for achieving a topological photonic crystal by using dielectric material," Phys. Rev. Lett. **114**(22), 223901 (2015).
34. Y. Yang and Z. H. Hang, "Topological whispering gallery modes in two-dimensional photonic crystal cavities," Opt. Express **26**(16), 21235–21241 (2018).
35. Z.-K. Shao, H.-Z. Chen, S. Wang, X.-R. Mao, Z.-Q. Yang, S.-L. Wang, X.-X. Wang, X. Hu, and R.-M. Ma, "A high-performance topological bulk laser based on band-inversion-induced reflection," Nat. Nanotechnol. **15**(1), 67–72 (2020).